Spectroscopic Evidence for a Substrate Dependent Orientation of Sexithiophene Thin Films Deposited onto Oriented PTFE

ARTICLE *in* THE JOURNAL OF PHYSICAL CHEMISTRY B · OCTOBER 1997

Impact Factor: 3.3 · DOI: 10.1021/jp9701303

4 AUTHORS, INCLUDING:

P. Lang
French National Centre for Scientific Research
81 PUBLICATIONS **1,814** CITATIONS
SEE PROFILE

Gilles Horowitz
French National Centre for Scientific Research
236 PUBLICATIONS **11,201** CITATIONS
SEE PROFILE

Fabien Garnier
Centre Hospitalier Universitaire de Limoges
207 PUBLICATIONS **7,060** CITATIONS
SEE PROFILE

Spectroscopic Evidence for a Substrate Dependent Orientation of Sexithiophene Thin Films Deposited onto Oriented PTFE

P. Lang,* G. Horowitz, P. Valat, and F. Garnier

Laboratoire des Matériaux Moléculaires, CNRS 2 rue H. Dunant, 94320 Thiais, France

J. C. Wittmann and B. Lotz

Institut Charles Sadron, 6 rue Boussingault, 67083 Strasbourg, France

Received: January 8, 1997[⊗]

Sexithiophene (6T) was deposited onto PTFE layers oriented by friction. The films were studied by polarized spectroscopy: UV−visible, IR absorption, and fluorescence. The nature of the surface and the deposition rate are shown to greatly influence the orientation of the molecules and the mesoscopic organization of the film. A quantitative analysis of the orienting influence of the PTFE substrate toward the structure of the molecular film is shown.

I. Introduction

Thiophene oligomers (nT) vacuum deposited onto various substrates present self-assembling properties that lead to highly organized semiconducting films possessing potential applications in thin film devices such as field-effect transistors (FET) and light-emitting diodes (LED).[1] The molecular orientation and the crystalline grain size have been shown to depend on both chemical structure of the constituting molecules and deposition parameters such as evaporation rate, pressure and substrate temperature, and thickness of the films.[2] The nature of the substrate also strongly affects the orientation of the molecules, the structure of the film, and accordingly the carrier mobility. In a previous work, we have shown that the molecular orientation is either parallel or normal to the surface, depending on the substrate.[3]

Recently, preliminary results with oligothiophenes and other conducting polymers suggested a good epitaxial relationship between the evaporated film and the PTFE substrate.[4] The structure of thin films of PTFE deposited by friction have already been analyzed and described notably by one of the authors.[5] The crystallized films formed of parallel, long, and straight ribbons are rather continuous and cover nearly all the glass surface (nearly 90%). Used as substrates, the films have a strong orienting effect along a unique direction relative to the substrate plane. They can induce either molecular epitaxy on the ribbons, which requires matching of crystallographic parameters, or graphoepitaxy,[5d] i.e. orientation of crystallites by the ribbons' edges. We report here how such PTFE films control the mesoscopic structure and orientation of sexithiophene films (6T, cf. Scheme 1) and optical properties of the film. We examine the orientation and the crystalline organization of the 6T films deposited at different deposition rates.

In a parallel paper,[6] we show by electron microscopy and electron diffraction on the same samples that a good epitaxial relationship exists at the 6T-oriented PTFE film interface, the *ac* or (010*)* plane of 6T crystals lying parallel to the (100) plane of the substrate (*a* and *c* are the long and short crystallographic axes of 6T crystal respectively[8]): the distance between the PTFE chains (0.56 nm) is very close to an intermolecular distance of 6T molecules (0.55 nm) (see Scheme 2a,b). The molecules have their long axis L parallel to the PTFE fibers and consequently

SCHEME 1: 6T Molecule and Its Molecular Axes

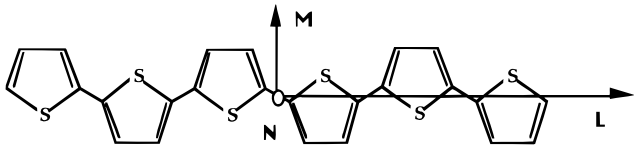

SCHEME 2: Position of 6T Molecules Epitaxially Deposited onto PTFE Substrates[a]

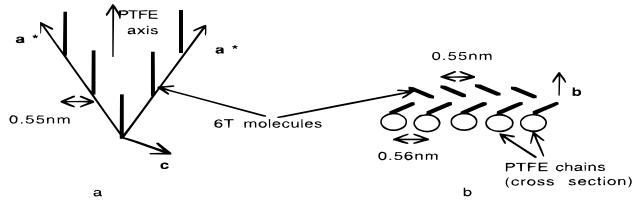

[a] Crystallographic axes *a*, *b*, *c* are relative to the 6T crystal; see ref 6.

the *a** axis (or, within less than 1°, the *a* axis) is tilted by ±23.5° with respect to the PTFE chain axis.

We compare here the spectroscopic data with the diffraction evidence. UV−vis, IR, and fluorescence spectra of 6T films deposited on orienting substrates allow one to examine molecules oriented along a unique direction in the substrate surface. The interpretation of UV−vis spectra is therefore greatly simplified in the present case and leads to the consideration that different molecular populations exist. Moreover, the nature and amount of poorly oriented molecules toward the PTFE chain axis can be evaluated.

II. Experimental Section

The 6T film preparation has been reported previously.[3] 6T films are evaporated at either low deposition rate (LDR) (≈0.1 Å/s) or high deposition rate (HDR) (≈10 Å/s).These samples are referred to hereafter as LDR and HDR. Their thicknesses were estimated between 30 and 60 nm from quartz microbalance measurements. A preliminary study of the effect of substrate temperature on the overall orientation of 6T molecules relative to PTFE chains has pointed out the interest of using low substrate temperature, i.e., 77 K. Accordingly, all the following experiments have been carried out at this temperature. The PTFE film preparation has been described elsewhere.[5a,b,6]

[⊗] Abstract published in *Advance ACS Abstracts,* September 1, 1997.

S1089-5647(97)00130-2 CCC: $14.00

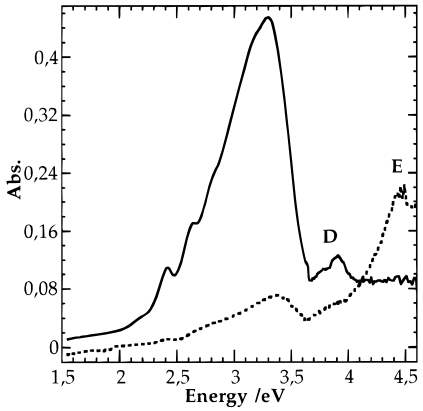

Figure 1. UV−vis absorption spectra at normal incidence of 6T/PTFE deposited at low rate (LDR): (—) $E_{||}$ to PTFE chains; (- - -) $E_{\perp}$ to PTFE chains.

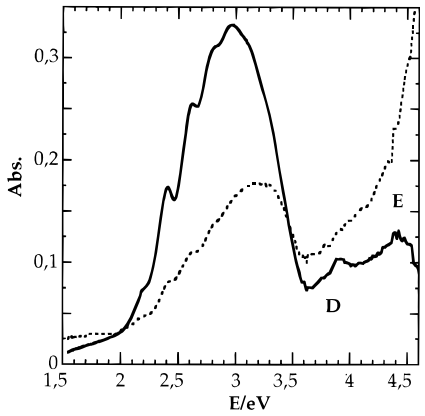

Figure 2. UV−vis absorption spectra at normal incidence of 6T/PTFE deposited at high rate (HDR): (—) $E_{||}$ to PTFE chains; (- - -) $E_{\perp}$ to PTFE chains.

Transmission UV−vis polarized spectra are recorded at normal or at 70° incidence angle on a Cary spectrometer equipped with a Glan-Taylor polarizer and a rotatable sample holder. The absorption of PTFE on a PTFE-coated glass slide is recorded under identical conditions as those of the reference. Before the deconvolution of spectra, the reflected light due to the film surface is partially eliminated by subtracting a base line taken outside the absorption range (λ > 650 nm) and extrapolated to the whole spectrum. Reflection IR spectra are recorded by using a Brucker IFS48 spectrometer at nearly normal incidence. Two polarizations have been used: p polarization where E_p is parallel to the incident plane (that containing the incident and reflected beams) and s polarization with E_s perpendicular to the same plane. In the quantitative analysis, only s-polarized spectra are considered. As shown in the Appendix for thin films and in the region where the substrate does not absorb light, the relative variation of the reflection coefficient $(R_s - R^{sub}{}_s)/R_s^{sub} = \Delta R_s/R_s$ is proportional to the absorption coefficient α.

The spectrofluorimeter (SLM AMINCO 8100) is equipped with a double and single monochromator at excitation and emission, respectively. The emission spectra are recorded at an excitation of 420 nm filtered by an interference filter also centered at 420 nm (band-pass 20 nm). The emitted light is filtered by a WG 495 nm long-pass filter (Schott). Excitation spectra are obtained by recording the emitted light at 590 nm, filtered with a WG 570 nm long-pass filter (Schott).

III. Results

III.1. UV−vis Spectroscopy. The polarized spectra at normal incidence of 6T films deposited at low (LDR) and high (HDR) deposition rates, are shown in Figures 1 and 2, respectively. The large difference in optical absorption as a function of light polarization reveals a strong molecular orientation.[6] All the observed bands within the range 1.55−4.1 eV appear L-polarized whereas band E located at 4.5 eV is M-polarized in agreement with the literature data.[2b,7] The dichroic ratio at normal incidence in the range 1.55−3.64 eV is defined by eq 1:

$$r^{\circ}_{vis} = (Abs^{\circ}_{||})/(Abs^{\circ}_{\perp}) \qquad (1)$$

where $Abs^{\circ}_{||}$ and $Abs^{\circ}_{\perp}$ are the integrated absorbances versus incident photon energy with E parallel and perpendicular to the PTFE chains, respectively. The dichroism is higher for the film deposited at low rate (Figure 1). The main feature of the spectra develops some shoulders on the low-energy side, which are usually assigned to vibronic replica associated with the C=C stretching vibration mode. Variations in the polarized spectra as a function of deposition rate are discussed in section IV.2. Figures 1 and 2 show s-polarized spectra of films deposited at low deposition rate and high deposition rate. It can be seen that the absorption band for LDR is asymmetric and relatively sharp with E_{max}= 3.3 eV, whereas for HDR, the shape is broader and rather symmetric with a maximum at a lower energy (E_{max}= 2.97 eV). Note that a significant dichroism is also observed for the two small L-polarized bands D_1 (3.78 eV) and D_2 (3.89 eV).

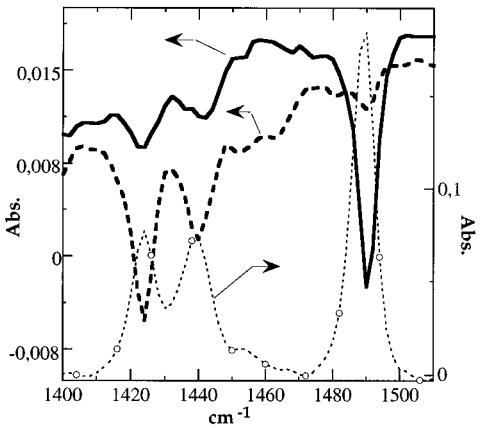

Figure 3. Reflexion IR polarized spectra of 6T/PTFE (LDR) in (C=C) stretching region: (—) $E_{||}$ PTFE chains; (- - -) $E_{\perp}$ PTFE chains and in the substrate plane; (- ○ -) 6T in KBr pellet.

The spectra recorded at an incident angle of 70° in all possible configurations of the electric field relative to the PTFE chains show an identical blue-shift and shape (figure not shown). Only the dichroic ratios are smaller at oblique incidence.

III.2. IR Spectroscopy. Previous studies have shown that the ν(C=C) vibration range 1550−1400 cm^{-1} provides interesting information about the molecular orientation, because it contains both L- and M-polarized bands. Moreover, these bands are not influenced by the crystalline field effect, in contrast to the low-frequency bands (within the range 900−600 cm^{-1}), which split into doublets.[8] Note that the bands of LDR and HDR films are located at the same frequencies.

Figure 3 shows a typical IR s-polarized spectra of the LDR 6T film ($E_{||}$ to the substrate plane). The L-polarized band at 1490 cm^{-1} (ν(C=C)) is strongly enhanced relative to the M-polarized bands at 1440 and 1426 cm^{-1} when the electric field **E** is parallel to the PTFE chains. This 1490 cm^{-1} band is much weakened when **E** is perpendicular to the PTFE chains. Similar observations are made for HDR films. These results confirm the favored orientation of the L molecular axis parallel to the PTFE chains. However, the presence of strong M-polarized bands with $E_{||}{}^{PTFE}$ shows that some molecules are

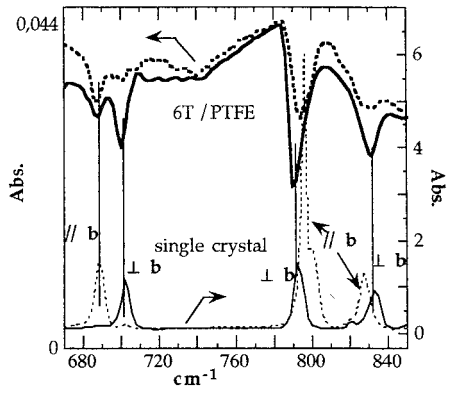

Figure 4. IR polarized spectra (LDR) in low/energy region: top (—) $E_{\perp}$ PTFE chains and in the substrate plane; (- - -) $E_{\parallel}$ PTFE chains; below, 6T single crystal (- - -) $E_{\parallel b}$; (—) $E_{\perp b}$.[8]

SCHEME 3: Experimental Configuration for Fluorescence Spectroscopy

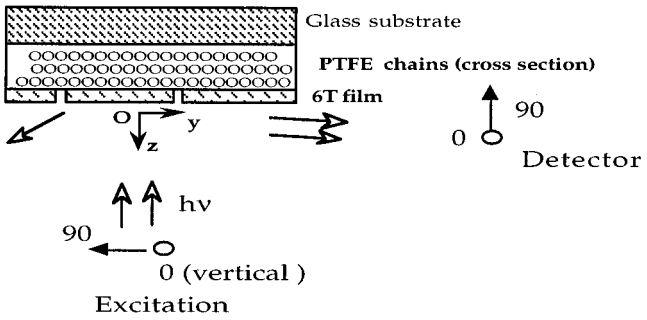

neither aligned along the PTFE chains nor lying on the substrate plane. The major part of these nonaligned molecules can be assumed to stand perpendicular to the substrate.

As in previous studies on single crystals,[8] the low-frequency region (Figure 4) shows some band splitting due to solid state interactions, as also observed in the visible spectrum. The frequencies of the split bands are very close to those of the single crystal ($\Delta\nu < 2$ cm^{-1}), i.e., the film and the single crystal appear to have the same crystalline structure[8b]), in agreement with electron diffraction data.[6] When the electric field **E** is in the substrate plane and normal to the PTFE chains, the *b*-polarized components of the doublets are weak, especially the one at 690 cm^{-1}, which has half the intensity of the *c*-polarized component at 705 cm^{-1}. The ratio ***b/c*** of ~1/2 is small compared to that (about 2) found in the spectrum of 6T in KBr pellets in which the molecules have no preferential orientation. This result indicates that a large proportion of molecules have their crystallographic *c*-axis in the plane of the substrate and perpendicular to the PTFE chains, in agreement again with electron diffraction data. The residual absorption of the *b*-polarized component comes both from molecules having their L-axis parallel to PTFE chains but deposited on the PTFE steps or ridges[6] and from molecules normal to the substrate. Similarly, when **E** is parallel to the PTFE chains, the *c*- and *b*-polarized bands are weak but not zero. The presence of these weak absorption bands, and particularly of the *b*-polarized one, irrespective of the electric field direction, confirms the presence of defects in the form of nonoriented molecules that are either tilted up from the substrate plane or located at the PTFE steps, in agreement with the above IR results and electron diffraction data.[6]

Finally, we have checked the nearly perfect orientation of PTFE by IR spectroscopy: we indeed observe that the bands of PTFE polarized normally to the chains at 1206 and 1150 cm^{-1} [9] are extremely weak when **E** is parallel to the PTFE chain,

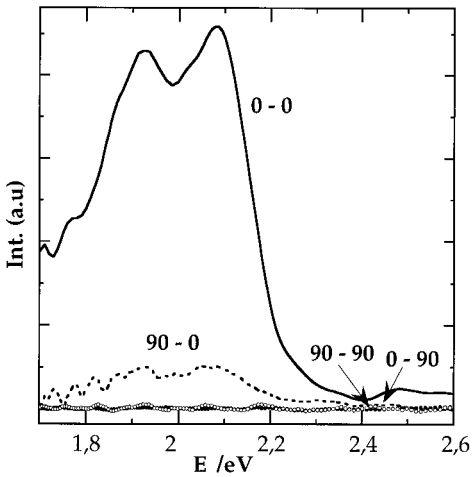

Figure 5. Polarized emission spectra of 6T/PTFE (LDR) ($\lambda_{exc} = 420$ nm or 2.95 eV); PTFE chains are vertical. Polarizers: 0, vertical; 90, horizontal.

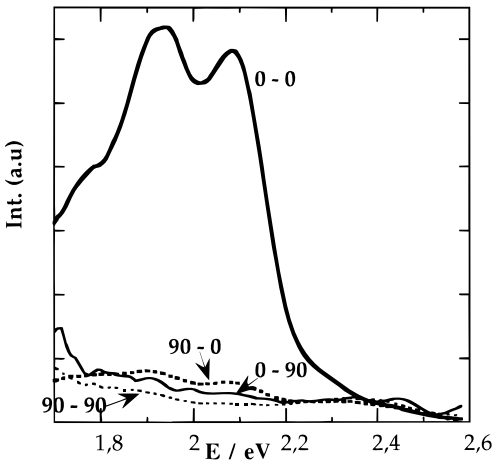

Figure 6. Polarized emission spectra of 6T/PTFE (HDR) ($\lambda_{exc} = 420$ nm or 2.95 eV); PTFE chains are vertical. Polarizers: 0, vertical; 90, horizontal.

i.e., less than 1% of the intensity measured when **E** is normal to the PTFE chains.

III.3. Fluorescence Spectroscopy. The PTFE chains are vertical, the substrate plane is at an angle close to 90° to the incident, beam and the detector is nearly in the substrate plane (see Scheme 3).

The polarized emission spectra for both deposition rates (Figures 5 and 6) show that emitted light is detected only when the incident and emitted electric fields are both parallel to the PTFE chains (spectrum 0−0). The other components (0−90) and (90−90) are close to zero (0 and 90 indicate vertical and horizontal polarization of the electric field, respectively, the PTFE chains are vertical; see Scheme 3). A weak emission is observed for the (90−0) configuration. We conclude that the molecules emitting light are rather aligned parallel to the PTFE chains.

The first peak at 1.9 eV is smaller for LDR than for HDR film.

The excitation spectra have been recorded in the (0−0) configuration (Figures 7 and 8). These spectra must be treated with care, because some parasitic diffusion could slightly disturb the measurements despite the use of filters. The vibronic replica appear mainly in these spectra.

In summary, the above spectroscopic data reveal that the long axis L orientation of the 6T molecules is mainly parallel to the PTFE chain axis. However, some disorientation exists, with 6T molecules perpendicular to the PTFE chains both in the

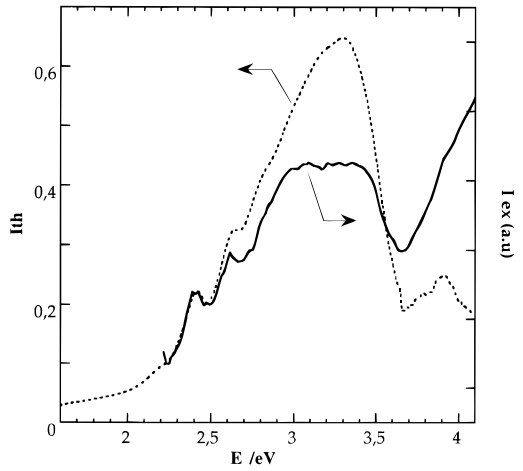

Figure 7. (—) Excitation spectrum 0-0 Iex of 6T/PTFE (LDR) λ_{emi} = 590 nm or 2.1 eV; (- - -) theoretical excitation Ith deduced from absorbance in figure 1. Ith = 1 − exp(−Abs ln 10); 0−0 is defined figure 5.

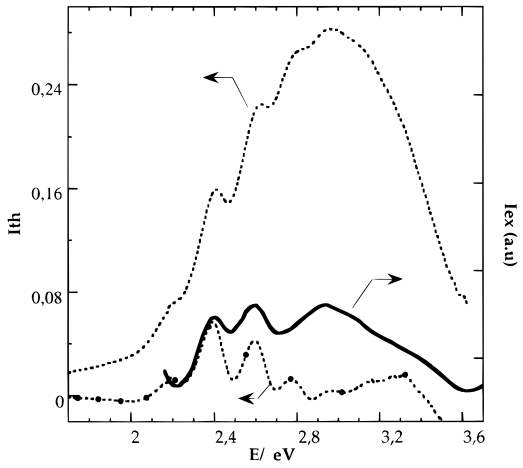

Figure 8. (—) Excitation spectrum 0−0 Iex of 6T/PTFE (HDR) λ_{emi} = 600 nm or 2.07 eV; (- - -) theoretical excitation Ith deduced from absorbance of figure 2. Ith = 1 −exp(−Abs ln 10). (- ● -) residual curve from figure 9a showing the A feature.

substrate plane and in a plane normal to this substrate. The shape of UV−vis spectra and the orientation depend on the deposition rate. In the next section, we develop a model of the molecular orientation and of the film composition in terms of molecular population.

IV. Modelization of Film Orientation

In this section, we present a quantitative determination of the film orientation and composition. The oligothiophene molecules assembled in the organic film are distributed in three populations of molecular fractions n_x, n_y, n_z, which have their long axis L parallel to x (PTFE chains axis), y, and z, respectively (see Scheme 2). The n_x and n_z populations indeed exist as shown previously,[6] whereas n_y takes into account the molecules poorly aligned along the y axis in the absorption spectra. These values can be deduced from the dichroic ratio (eq 1) and average angular functions $tg^2\ \theta$ and $\cos^2\beta$, where θ and β are defined for a single molecule in Scheme 4.

$$n_y/n_x = \langle tg^2\ \theta\rangle = 1/r^\circ \quad (2)$$

$$n_z = \langle \cos^2\beta\rangle \quad (3)$$

IV.1. Evaluation of n_y/n_x from UV−vis and IR Spectroscopies. Taking into account the dichroic ratios r°_{IR} and

SCHEME 4

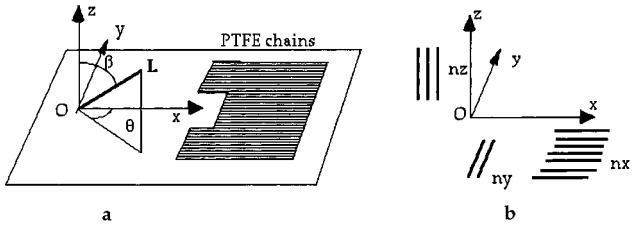

TABLE 1: Comparison of Dichroic Ratio and n_y/n_x Calculated from both IR and Vis Data

		LDR[a]	HDR[b]
vis	r°_{vis}	8.4	2
	n_y/n_x	0.12 ± 0.02	0.52 ± 0.1
IR	r°_{IR}	8	4.6
	n_y/n_x	0.12 ± 0.02	0.22 ± 0.04

[a] Film formed at low deposition rate. [b] Film formed at high deposition rate.

r°_{vis} (eq 1), the molecular ratio n_y/n_x can be calculated (Table 1). The measured ratio n_y/n_x is small for both rates, particularly when the oligomer film is deposited at low rate, confirming that the film is well oriented. The values calculated from UV−vis and IR spectroscopies are identical for LDR but differ significantly for the HDR film.

The latter discrepancy suggests that the two spectroscopies do not probe exactly the same species. In contrast to IR vibrational transitions, electronic transitions are associated not only with isolated molecules but also with dimers, aggregates, and crystals in which intermolecular interactions take place.[10,2,11,14]

To analyze further the structural and electronic properties of oligomer films, some issues on the UV−vis absorption spectra of oligothiophenes must taken into account that make it possible to rationalize the spectra through their deconvolution.

IV.2. Deconvolution of UV−vis Spectra. *IV.2.1. General Concepts.* Quantum chemistry calculations have shown that the molecular levels in sexithiophene consist of a $1A_g$ ground state, followed by a $1B_u$ and a $2A_g$ excited state.[2a,j,k,20] It is generally agreed that the $1B_u$ level is at a lower energy than the $2A_g$ level. For a one photon absorption, the $1A_g \rightarrow 1B_u$ transition is symmetry allowed, whereas the $1A_g \rightarrow 2A_g$ is symmetry forbidden. In solution, the molecule is free to rotate around the intercycle C−C bonds, and its visible absorption shows a wide band centered at 430 nm that is practically independent of solvent. This band corresponds to the $1A_g \rightarrow 1B_u$ transition, followed by three sharper bands in the UV region. When the molecule is rigidified in a polymer matrix, the absorption is red-shifted, and the shape of the wide band changes to a structured spectrum constituted by regularly spaced peaks of decreasing intensity, which are interpreted as vibronic replica of the $1A_g \rightarrow 1B_u$ electronic transition.[17,11g]

In thin solid films, the UV−visible absorption is once more completely reshaped by the coupling between the transition dipole moments of the molecules,[2,11,14,17] which are aligned along the L axis, and are therefore all parallel to each other in sexithiophene crystals. Because the coupling of the transition dipole moment is very strong in sexithiophene, the effect of this feature is a splitting of the $1B_u$ level into a wide exciton band, the width of which has been estimated, from the magnitude of the transition dipole moment and the intermolecular spacing, to be between 10 000 and 15 000 cm^{-1} (i.e., more than 1 eV). In turn, the k selection rule states that one-photon-induced transitions are only allowed at $k = 0$. In the case of concern, the allowed transition is directed toward the *top* of the $1B_u$ exciton band inducing a blue-shift of the $1A_g \rightarrow 1B_u$ transition. The expected shape of the absorption spectrum

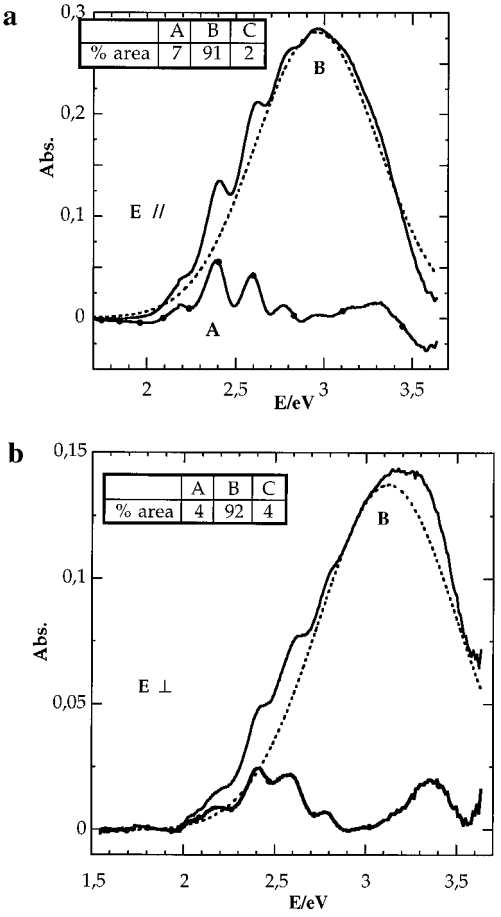

Figure 9. (a) Deconvolution of exptl curve (—) of figure 2 (HDR) by a Gaussian curve (B) (- - -); (— ● —) residue (exptl − calcd). (b) Idem as for (a) but relative to the exptl curve (—) of Figure 2 (see dotted line with $E_\perp$ PTFE chains).

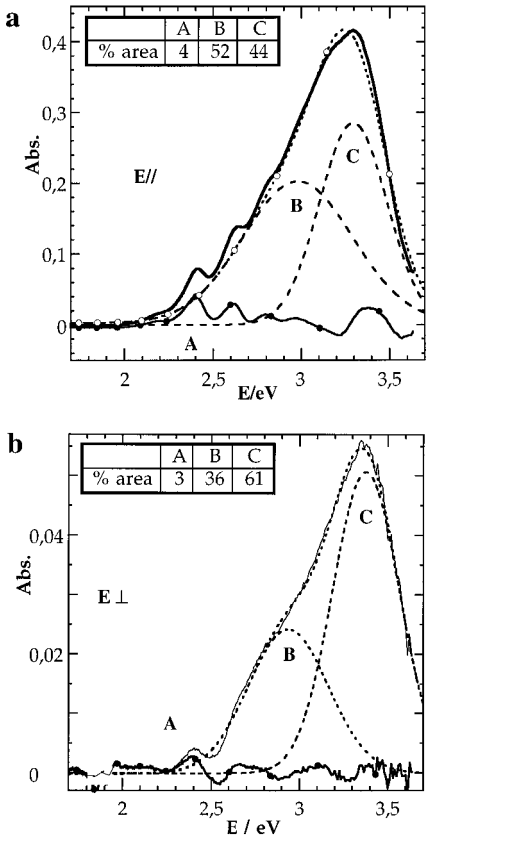

Figure 10. (a) Deconvolution of exptl curve (—) of Figure 1 (LDR) by two Gaussian curves B,C (- - -), with their sum (- - ○ - -); (— ● —) residue (exptl −calcd). (b) Idem as for (a) but for $E_\perp$ PTFE chains.

would therefore consist of a sharp peak with a steep decrease at the high-energy side and a smoother slope at the low-energy side. Such a feature, which we name C, is indeed observed in spectra of LDR films (see Figure 1)—together with feature B that is described below. The corresponding peak, located at 3.35 ± 0.1 eV, indicates the upper edge of the $1B_u$ exciton band. Although it is predicted that feature C would display a slightly asymmetrical form, we shall approximate it to a Gaussian curve. Indeed, we have chosen such a symmetric curve since another feature occurs at the low-energy side (see below feature B).

HDR films present a second feature, called B, which consists of a wide band centered at around 3 eV. As a direct correlation can be made between the size of the grains and the deposition rate,[6,2c,e] we can attribute this feature to the presence in HDR films of very small grains, in which the width of the exciton band is reduced. According to Hochstrasser and Kasha, the total exciton bandwidth is given by $\Delta E \approx G\mu^2/d^3$ where G is a geometrical factor, μ the intensity of transition dipole moment and d the distance between molecular centers. G varies from $2(3\cos^2\theta - 1)$ for a dimer[10] to 8.4 $(3\cos^2\theta - 1)$ for an infinite two-dimensional crystal[11] (which apply for a 6T large grain); therefore, ΔE may vary by a factor of 4 and feature B can be ascribed to a distribution of grain size (θ is an angle relative to the molecule orientation). Because of the statistical distribution of the size of these microcrystals, it can be reasonably assumed that this B feature will have a Gaussian shape. We note that feature B could alternatively be attributed to surface effects, in which molecules close to the surface of the grains would present similar characteristics as molecules in microcrystals, leading to the narrowing of ΔE. In that case, the correlation between the size of the grains and the intensity of feature B would result from the variation of the surface to volume ratio, which indeed increases as the size of the grains decreases.

A third feature (A) appears at the low-energy side of the spectrum. It consists of a series of regularly spaced bands of low intensity, which recalls the shape of the absorption of the isolated molecule A_{iso} rigidified in a polymer matrix.[2b,17] A differs however from A_{iso} by the much lower intensity of the peaks.[19] A is also less intense than both B and C. Following a model derived from an analysis of the photoluminescence of sexithiophene solid films,[14a] we attribute this A feature to the $1A_g \rightarrow 2A_g$ forbidden transition, which is made partially allowed by a coupling between the electronic transition and an *ungerade* (antisymmetrical) vibronic transition. We note that in this model, the first (partially) allowed transition is a 0−1 transition; the pure $1A_g \rightarrow 2A_g$ (0−0) transition is absent or very weak. The latter has been reported at 2.27 eV from the measured two-photon excitation spectrum of 6T crystals whereas the first peak of the vibronic progression of feature A is located at 2.39 eV.

IV.2.2. Deconvolution of the Spectra. The above analysis has been used for the deconvolution of the spectra of LDR and HDR films.

In the HDR spectrum (Figure 2), C is very small and the spectrum was resolved as a single Gaussian curve (Figure 9a,b). The residual curve clearly exhibits the bands corresponding to feature A and also a feature at the high-energy side that would indicate the presence of feature C. The LDR spectrum in Figure 1 could be fitted with two Gaussian curves. The residual curve (i.e., the difference between the measured and the calculated curves, Figure 10a) presents a feature at the low-energy side that corresponds to feature A and a bump at high energy (3.4 eV), which we could attribute to the inherently asymmetrical character of feature C.

The above treatment allows us to estimate the respective contributions of A, B, and C in each spectrum together with

TABLE 2: Dichroic Ratio r° and n_y/n_x for A,B, and C Features Deduced from Deconvolution of Polarization (See Figures 9 and 10)

	LDR[a]			HDR[b]		
	A	B	C	A	B	C
$r^\circ_{vis} \pm 20\%$	≈10	13	5	3.3	1.85	≈1
$n_y/n_x \pm 20\%$	≈0.1	0.08	0.16	0.31	0.53	≈1

[a] Film deposited at low rate. [b] Film deposited at high rate.

the corresponding dichroic ratio. Table 2 shows that both the dichroic ratio and the area ratio of B to C depend on the polarization in both films; similar conclusions were already drawn for 6T on glass.[2c,13] This supports our analysis according to which there are indeed two independent features B and C (particularly in the LDR film) we attribute to two different crystalline populations.

Estimation of Oscillator Strength Ratios f_B/f_C and f_B/f_D. Oscillator strength ratios are estimated on the basis of the absorption of the weak bands D_1 and D_2 located at ca. 3.3 eV. These bands are obviously L-polarized. Assuming that the absorption at 3.3 eV in the spectrum polarized parallel to the PTFE chains is proportional to the total number of molecules oriented parallel to PTFE chains, $n^t_{||}$, taken as equal to the sum $(n^B_{||} + n^C_{||})$. We calculate the oscillator strength ratio as

$$f_B/f_C = 2.2 \pm 0.4$$

This value is in good agreement with that given in ref 11h, which was estimated from two spectra that approximately contain only either B or C. The recalculated value of n_y/n_x is 0.13 for LDR (instead of 0.12) and does not change for HDR.

Similarly, the ratio f_B/f_D is:

$$f_B/f_D \approx 15-20$$

The oscillator strength f_D of the transition D is as expected, relatively small since the crystalline field effect on the location of D is very small. The value of f_B/f_D is much larger than that given in ref 12.

IV.3. Orientation along the Three Axes As Estimated by IR Spectroscopy. The presence of M-polarized molecular bands in the IR spectra allows us to calculate the number n_z of molecules perpendicular to the substrate. By analogy with the previous quantitative approach,[3a] we define the ratio R(C═C):

$$R(\text{C═C}) = \text{Abs(L)/Abs(M)} \quad (4)$$

where Abs(L) and Abs (M) are the integrated pseudoabsorption under s-polarization of the L-polarized band (area under the band in the 1480−1510 cm^{-1} range) and the absorption of the two M-polarized bands (area in the 1400−1480 cm^{-1} range), respectively. This ratio was shown to be proportional to the absorption coefficients and transition moments for both transitions (see Appendix); it can thus be evaluated for both spectra with $E_{||}$ to PTFE chains i.e., $R_{||}$(C═C), and $E_\perp$ to PTFE chains, i.e., $R_\perp$(C═C) and for the spectrum of isotropic 6T dispersed in KBr pellet, i.e., R_b(C═C). We assume that, as shown by the electron diffraction study,[6] the n_x population has its molecular plane tilted by $\delta/2 = 33°$ to the substrate plane. d is the angle between the molecular planes in the herringbone structure, i.e., 66°.[8] Using the same methodology as described in ref 3a we calculate:

$$n_y/n_x = \langle \text{tg}^2\,\theta_{IR}\rangle = \frac{R_\perp\left(\cos^2\frac{\delta}{2} + \frac{R_b}{R_{||}}\right)}{\frac{R_\perp}{2} + R_b} \quad (5)$$

$$n_z = \langle \cos^2\beta\rangle \frac{2R_b^{\,2} - R_\perp R_{||}\cos^2(\delta/2)}{\left(R_b + \frac{R_\perp}{2}\right)(2R_b + R_{||})} \quad (6)$$

$$n_x = \frac{R_\perp R_{||}(1/2 + \cos^2(\delta/2)) + R_b(R_\perp + R_{||})}{(2R_b + R_{||})\left(R_b + R_\perp\left(1/2 + \cos^2(\delta/2) + \frac{R_b}{R_{||}}\right)\right)} \quad (7)$$

$$n_y = 1 - n_z - n_x \quad (8)$$

Table 3 gives the values n_x, n_z, n_y, and n_y/n_x for both deposition rates, which can be compared with those in Table 1: the ratios n_y/n_x calculated by both methods from IR data are in good agreement, which supports the relevance of our model. They confirm that the orientation of the molecules are mostly parallel to the PTFE fibers but that the end-on molecules n_z are nevertheless important, particularly for HDR. It is worth noting that the contribution of molecules directly deposited on the bare glass surface (∼10%) is included in this value.

IV.4. Orientation and State of Emitting Molecules. The ratio of n_y/n_x is deduced from the emitted light W (Figures 5 and 6) and usual equations.[21] The subscript f refers only to those molecules that emit light.

$$n_{yf}/n_{xf} = \langle \text{tg}^2\,\theta_f\rangle = W(90-0)/W(0-0)$$

and the numerical values are

$$n_{yf}/n_{xf}(\text{LDR}) \sim 0.11 \qquad n_{yf}/n_{xf}(\text{HDR}) \sim 0.07$$

The value for LDR film is in good agreement with IR and UV−vis data. However, a smaller value is observed for HDR film suggesting structural differences between oriented and nonoriented molecules toward the PTFE chain axis.

The excitation spectra (Figures 7 and 8) do not follow the theoretical spectra deduced from the absorption, except within the region 2.2−2.5 eV. Accordingly, feature A is mainly responsible for the fluorescence, in agreement with the literature.[2b,11f,14,17] B and C are very weak.

To summarize, both IR and UV−vis spectroscopies provide quantitative information on the orientation of the 6T molecules. A large proportion of them (n_x) is oriented parallel to the PTFE chains, whereas some misaligned molecules appear to be normal to the PTFE chains either out of the substrate plane (n_z) or, for a few of them, in this plane (n_y). The UV−vis spectra, whose shape depends on the deposition rate, have been decomposed into three features that originate from the different molecular populations, i.e., from molecules having different environments.

V. Discussion

First we shall compare and discuss the present spectroscopic results to those obtained by electron diffraction.[6] Electron diffraction data gave evidence for three observed crystalline populations differing by their molecular orientation (6T long axis L and molecular plane orientation). In two of these, L is oriented parallel to the PTFE chain axis, but as a consequence of a different level of substrate/deposit interactions, the molecular plane orientations relative to the substrate are different.[6] These two populations are gathered in n_x. The strongest, epitaxial interactions lead to a symmetric, herringbone-type

TABLE 3: Molecular Ratios Calculated from IR Data and Equations 5−8

	LDR[a]	HDR[b]
n_x	50%	35%
n_z	44%	59%
n_y	6%	6%
n_y/n_x	0.12	0.17

[a] Deposition at low rate. [b] Deposition at high rate.

arrangement with the molecular planes tilted by ±33° to the film plane. The less specific interactions that probably occur at the PTFE film edges or ridges give rise to an orientation that can be considered as more defective and in which the molecular plane of half of the 6T molecules is normal to the film surface (given the crystal structure the other half is tilted by 24° to that surface). Finally, in the most "defective" third population the long axis L (and the molecular plane) is oriented nearly normal to the film plane. This population, which is part of the n_z population, does not experience any orienting influence of PTFE. Although the latter population was observed with both techniques, our data do not allow us to determine their location with respect to the substrate. We believe, however, that the orienting effect of PTFE is lost for 6T thicknesses above a certain value.

Further comparisons between data deduced from the two techniques are difficult because of the different sampling procedures and observed objects. In this respect, the optical spectroscopies are more reliable since they average over much larger areas of the sample (ca. 1 mm^2 for optical probes and about 10 μm^2 for electron diffraction).

As far as the vis spectra are concerned, all the components within the range 2−3.5 eV are L-polarized. Note that in single crystals, some bands likely M-polarized, appear also in this spectral domain at frequencies slightly different from the L-polarized ones, but are at least 10 times weaker than the L-polarized bands;[18,22] they cannot be detected in oriented films with some defects.

The shape of the UV−vis spectra and their polarization dependence can be rationalized by three features A, B, and C. The dichroic ratio is higher for B than for C, indicating that feature (B) is not simply related to orientational disorder as suggested in refs 2j, 11h,15, and 16. The presence of C is preferentially observed at a low deposition rate as found on glass or quartz substrates. A low deposition rate favors large crystallites as shown by microscopic observations.[6,2c,13] Feature C is associated to these large grains. In contrast, for high deposition rates (HDR), the spectrum is dominated by the broad band B centered at 2.95 eV (420 nm) because of the presence of small crystallites. We believe that B and C bands are the spectroscopic signatures of two different molecular populations that have different surroundings, either in grains of difference sizes or between molecules at the surface and in the bulk of the same grain. Recent data of ellipsometry obtained with the single crystal of 6T[23] would confirm this interpretation: a single, sharp, and quite symmetric band is revealed around 3.6 eV, indicating a single population of molecules.

Although the present explanation provides a simple rationale, it does not rule out a possible influence of the crystallite shape[11a,24] that could well vary with the deposition rate.

Concerning the comparison of spectroscopic data, we recall that the signal given by a molecule may have different origins. Fluorescence is the most "restrictive" one and probes only the strongly oriented light-emitting molecules. IR spectroscopy in the 1500 cm^{-1} range provides information at the molecular scale, whereas UV−vis spectroscopy is sensitive to mesoscopic organization and to solid-state effects. This could account for the small differences between results obtained with the latter techniques. However, the matter needs to be investigated further, in particular regarding the physical origin of (B) and (C) features in the UV−vis spectra.

VI. Conclusion

The present spectroscopic studies demonstrate the important alignment effect of oriented PTFE layers on vacuum-deposited 6T films and the resulting impact on their optical properties. They provide a convenient and global measurement of the 6T crystal populations. As a rule, the 6T molecular and PTFE chain axis are, in agreement with electron diffraction results, parallel to each other. However, a fraction of "misaligned" molecules toward the orienting substrate exists in all films investigated whether 6T is deposited at low or high rates. The optical spectroscopies underline the importance of the latter population (molecules aligned along PTFE edges and nearly normal to the substrate plane irrespective of the PTFE axis) relative to the well-oriented crystal population (epitaxy on PTFE).

As with glass substrates, the deposition at high rate leads to a broad feature in the UV−vis spectra, associated with a small crystal size whereas that at low rate results in a higher fraction of aligned 6T molecules and leads to a sharper UV−vis feature associated with the presence of grains of larger size. This result has been analyzed in terms of two molecular populations B and C that have different surroundings.

Acknowledgment. We gratefully acknowledge the supply of sexithiophene by Dr. A. Yassar. We thank Dr. B. Desbat and T. Buffeteau for stimulating discussions.

Appendix. Relationship between Reflectance and Absorption Coefficients. In this calculation, we consider a three-film model, air/ film/substrate, in which the substrate is isotropic (complex index $\hat{n}_{sub}$) and the film uniaxial ($\hat{n}_{xy}$, $\hat{n}_z$). From refs 25 and 26, the reflectance is given for a thin film ($d \ll \lambda$) by

$$R_s - R_s^{sub} = R_s^{sub} 8\pi \frac{d}{\lambda} \cos\phi \, \mathrm{Im}\left(\frac{\hat{n}_{xy}^{\,2} - \hat{n}_{sub}^{\,2}}{\hat{n}_{sub}^{\,2} - 1}\right) \quad \text{(A1)}$$

in which R_s and R_s^{sub} are the reflectances for the system (film + substrate) and the substrate, respectively. ϕ is the incidence angle.

Assuming a little absorbing substrate, $n_{sub}^2 \gg k_{sub}^2$, it follows that

$$R_s - R_s^{sub} = R_s^{sub} 8\pi \frac{d}{\lambda} \frac{\cos\phi}{\hat{n}_{sub}^{\,2} - 1}\left[\mathrm{Im}(\hat{n}_{xy}^{\,2}) + \frac{1 - \mathrm{Re}(\hat{n}_{xy}^{\,2})}{\hat{n}_{sub}^{\,2}} \mathrm{Im}(n_{sub}^{\,2})\right] \quad \text{(A2)}$$

Re and Im correspond to the real and imaginary parts.

Limiting ourselves to the region where the substrate is not absorbing, eq A2 becomes

$$R_s - R_s^{sub} = R_s^{sub} 8\pi \frac{d}{\lambda} \frac{\cos\phi}{\hat{n}_{sub}^{\,2} - 1}(2 n_{xy} k_{xy}) \quad \text{(A3)}$$

or

$$(R_s - R_s^{sub})/R_s^{sub} = 8\pi \frac{d}{\lambda} \frac{\cos\phi}{\hat{n}_{sub}^{\,2} - 1}(2 n_{xy} k_{xy}) = -\mathrm{Abs}_s$$

Since the relative variations of R_s are small, this quantity with a minus sign is usually called the pseudoabsorbance Abs_s.

In the (C═C) stretching band region, n_{xy} variation is small (only a few percent) and its variation compensates in the integration domain of the band:

$$\int_{\upsilon_2}^{\upsilon_1} n_{xy}\, k_{xy}\, \mathrm{d}\upsilon \sim \langle n_{xy} \rangle \int_{\upsilon_2}^{\upsilon_1} k_{xy}\, \mathrm{d}\upsilon$$

Hence n_{xy} can be considered as a constant in eq A3. The ratio for two near bands is

$$\mathrm{Abs}(1)/\mathrm{Abs}(2) \approx \frac{\lambda(2)\, k_{xy}(1)}{\lambda(1)\, k_{xy}(2)} \approx \frac{\alpha(1)}{\alpha(2)} \qquad \text{(A4)}$$

$\alpha(i)$ is the absorption coefficient of the band i.

Remark: In the case of an anisotropic substrate with indices in its plane ($\hat{n}_{\mathrm{sub},x}$; $\hat{n}_{\mathrm{sub},y}$) and when the electric is parallel to *x* or *y* axes, $\hat{n}_{\mathrm{sub}}$ must be replace by $\hat{n}_{\mathrm{sub},x}$ and $\hat{n}_{\mathrm{sub},y}$, respectively. Equation A4 is unchanged.

References and Notes

(1) See, for example: (a) Burroughes, J. H.; Jones, C.; Friend, R. H. *Nature*, **1988**, *335*, 137. (b) Assadi, A.; et al., *Appl. Phys. Lett.* **1988**, *53*, 1995. (c) Horowitz, G.; et al. *J. Mol. Electron.* **1991**, *7*, 85. (d) Burroughes, J. H.; et al. *Nature* **1990**, *341*, 539. (e) Braun, D.; Heeger, A. J. *Appl. Phys. Lett*. **1991**, *58*, 1982. (f) Garnier, F.; Yassar, A.; Hajlaoui, R.; Horowitz, G.; Deloffre, F.; Servet, B.; Ries, S.; Alnot, P. *J. Am. Chem. Soc.* **1993**, *115*, 8716 and references therein.

(2) (a) Lazzaroni; R.; Pal, A. J.; Rossini, S.; Ruani, G.; Zamboni, R.; Taliani, C. *Synth. Met*. **1991**, *42*, 2359. (b) Egelhaaf, H. J.; Bäuerle, P.; Rauer, K.; Hoffmann, V.; Oelkrug, D. *J. Mol. Struct.* **1993**, *293*, 249; *Synth. Met*. **1993**, *61*, 143. (c) Servet, B.; Horowitz, G.; Ries, S.; Lagorsse, O.; Alnot, P.; Yassar, A.; Deloffre, F.; Srivastava, P.; Hajlaoui, R.; Lang, P.; Garnier, F. *Chem. Mat*. **1994**, *6*, 809. (d) Hamano, K.; Kutata, T.; Kubota, S.; Koezuka, H. *Jpn. J. Appl. Phys.* **1994**, *33*, L1031. (e) Lovinger, A. J.; Davis, D. D.; Ruel, R.; Torsi, H. E.; Dodabalapur, A.; Katz, L. *J. Mater. Res.* **1995**, *10*, 2958. (f) Lovinger, A. J.; Davis, D. D.; Dodabalapur, A.; Katz, H. E.; Torsi, L. *Macromolecules* **1996**, *29*, 4952. (g) Muller, H.; Petersen, J.; Strohmaier, R.; Gompf, B.; Eisenmenger, W.; Vollmer, M. S.; Effenberger, F. *Adv. Mater*. **1996**, *8*, 733. (h) Soukopp, A.; Glockler, K.; Bauerle, P.; Solkolowski, M.; Umbach, E. *Adv. Mater*. **1996**, *8*, 902. (i) Nardelli, M. B.; Cvetko, D.; Derenzi, V.; Gotter, R.; Morgante, A.; Peloi, M.; Tommasini, F.; Danielli, R.; Rossini, S.; Taliani, C.; Zamboni, R.; *Phys. Rev. B: Condens. Matter* **1996**, *53*, 1095. (j) Kanemitsu, Y.; Shimizu, N.; Suzuki, K.; Shiraishi, Y.; Kuroda, M. *Phys. Rev. B* **1996**, *54*, 2198. (k) Taliani, C.; Blinov, L. M. *Adv. Mater*. **1996**, *8*, 353.

(3) (a) Lang, P.; Hajlaoui, R.; Garnier, F.; Desbat, B.; Buffeteau, T.; Horowitz, G.; Yassar, A. *J. Phys. Chem*. **1995**, *99*, 5492. (b) Lang, P.; Hajlaoui, R.; Dallas, J. P.; Garnier, F.; Yassar, A.; Horowitz, G. *J. Chim. Phys.* **1995**, *92*, 967. (c) Lang, P.; Ardhaoui, M. E.; Wittmann, J. C.; Dallas, J. P.; Horowitz, G.; Lotz, B.; Garnier, F.; Straupe, C. *Synth. Met.* **1997**, *84*, 605.

(4) (a) Wittmann, J. C.; Smith, P. *Nature*, **1991**, *352*, 414. (b) Wittmann, J. C.; Lotz, B.; Smith, P. *Prog. Colloid Polym. Sci*. **1993**, *92*, 32. (c) Schott, M.; *Synth. Met.* **1994**, *67*, 55. (d) Smith, H. I.; Geis, M. W.; Thompson, C. V.; Atwater, H. A. *J. Cryst. Growth 1980*, *63*, 527.

(5) (a) Yang, C. Y.; Yang, Y.; Hotta, S. *Synth. Met.* **1995**, *69*, 303. (b) Fahlma, M.; Rasmusson, J.; Kaeryama, K.; Clark, D. T.; Beamson, G.; Salaneck, W. R. *Synth. Met.* **1994**, *66*, 123. (c) Lang, P.; Valat, P.; Horowitz, G.; Garnier, F.; Yassar, A.; Wittmann, J. C.; Lotz, B.; Meyer, S. *J. Chim. Phys.* **1995**, *92*, 963. (d) Gills, R.; Hadziannou, G.; Lang, P.; Garnier, F.; Wittmann, J. C. *Adv. Mater*. **1997**, *9*, 331.

(6) Wittmann, J. C.; Lotz, B.; Straupe, C.; Lang, P.; Horowitz, G.; Garnier, F. *Thin Solid Films* in press.

(7) Yassar, A.; Horowitz, G.; Wintgens, V.; Valat, P.; Hmyene, M.; Deloffre, F.; Srivastava, A.; Lang, P.; Garnier, F. *J. Phys. Chem.* **1995**, *99*, 9155.

(8) (a) Horowitz, G.; Bachet, B.; Yassar, A.; Lang, P.; Demanze, F.; Fave, J. L.; Garnier, F. *Chem. Mater*. **1995**, *7*, 1337. (b) Rabolt, J.; Burns, F. C.; Schlotter, N. E.; Swalen, J. D. *J. Chem. Phys.* **1983**, *78*, 946.

(9) Cutler, D. J.; Hendra, P. J.; Rakalka, R. R.; Curby, M. E. A. *Polymer*, **1981**, *22*, 726.

(10) Pope, M.; Swenberg, C. E. *Electronic Processes in Organic Crystals*; Oxford University Press: New York, 1982.

(11) (a) Hochstrasser, R. M.; Kasha, M. *Photochem. Photobiol*. **1964**, *3*, 317. (b) Kuhn, H. *Spectroscopy of Monolayers Assemblies*; In Weissberger, A.; Rossiter, B. W., Eds.; Physical Methods of Chemistry 1: Wiley-Interscience: New York, 1972, Part IIIB, p 593. (c) Nolte, H. J.; Buss, V.; *Chem. Phys. Lett*. **1973**, *19*, 395. (d) Schoeler, U.; Tews, K. H.; Kuhn; H. *J. Phys Chem.* **1974**, *61*, 5009. (e) Nakahara, H.; Nakayama, J.; Hoshino, M.; Fukuda, K. *Thin Solid Films*, **1988**, *160*, 87. (f) Bondarev, S. L.; Ivanov, I. I.; Romashin, Y. N.; Kulinkovich, O. G. *Zh. Prikl. Spekt*. **1992**, *56*, 739. (g) Bongiovanni, G.; Botta, C.; Di Silvestro, G.; Mura, A.; Tubino, R. *Phys. Lett.* **1995**, *A208*, 165. (h) Egelhaaf, H.-J.; Oelkrug, D. *Proc. SPIE* **1995**, *2362*, 398.

(12) Oeter, D.; Egelhaaf, H.-J.; Ziegler, Ch.; Oelkrug, D.; Göpel, W. *J. Chem. Phys*. **1994**, *101*, 6344.

(13) Hajlaoui, R. Ph.D. Thesis, Rouen, 1995.

(14) (a) Deloffre, F.; Garnier, F.; Srivastava, P.; Yassar, A.; Fave, J. L. *Synth. Met*. **1994**, *67*, 223. (b) Oeda, Y.; Nishi, O.; Matsushima, Y.; Mizuno, K.; Matsui, A. H.; Michinomae, M.; Takeshima, M.; Goto, T. *Chem. Phys*. **1996**, *213*, 421 and references therein.

(15) Niko, A.; Meghdadi, F.; Ambrosch-Draxl, C.; Vpgl, P.; Leising, G. *Synth. Met.* **1996**, *76*, 177.

(16) Oelkrug, D.; Egelhaaf, H.-J.; Haiber, J. *Thin Solid Films*, in press.

(17) (a) Tubino, R.; Mura, A.; Bosisio, R.; Botta, C.; Di Silvestro, G. *Mater. Res. Soc. Proc.* **1996**, *413*, 491. (b) Botta, C.; Bosiso, R.; Bongiovanni, G.; Mura, A.; Tubino, R. ICSM 96, Salt Lake City, UT, *Proceedings of Synthetic Met*als, in press.

(18) Mucini, M.; Lunedei, E.; Taliani, C.; Garnier, F.; Baessler, H. ICSM 96, Salt Lake City, UT, *Proceedings of Synthetic Metals* in press.

(19) From the density and thickness of the film, we have estimated the molar exctinction coefficient of feature A to ca. 3000 $\mathrm{mol}^{-1}\cdot\mathrm{cm}^2$, which is more than 10 times lower than that of 6T in solution or isolated in a polymer matrix; (see ref 17 and Colditz, R. Grebner, D.; Helbig, M.; Rentsch, S. *Chem. Phys*. **1995**, *201*, 309.

(20) Periasamy, N.; Danieli, R.; Ruani, G.; Zamboni, R.; Taliani, C. *Phys. Rev. Lett.* **1992**, *68*, 919.

(21) Long, D. A. *Raman Spectroscopy*; McGraw-Hill Int. Book Company: New York, 1977.

(22) Horowitz, G.; Delannoye, P.; Lang, P.; Valat, P.; Garnier, F. "JPC 96" meeting, Collonges-la-Rouge, France, 1996.

(23) Lang, P.; et al. Unpublished data.

(24) (a) Stein, R. S. *J. Polym. Sci.* **1969**, *A-2,7*, 1021. (b) Bottcher, C. J. F.; *Theory of Electric Polarization* 2nd ed.; Elsevier: Amsterdam, 1973; Vol. 1. (c) Hunderi, O. *Phys. Rev.* **1973**, *B7*, 3419. (d) Abeles, F.; Borensztein, Y.; Lopez-Rios, T. *Advances in Solid State Physics*—Festköperproblem; Grosse, P., Ed.; Vieweg: Braunschweig, 1984; Vol. 24, p 93. (e) Harbraken, F. H. P. M.; et al. *Surf. Sci*. **1980**, *96*, 345.

(25) (a) Heavens, O. S. In *Optical Properties of Thin Solid Films*; Butterworths: London, 1955. (b) Yen, Y. S.; Wong, J. S. *J. Phys. Chem*. **1989**, *93*, 7208.

(26) Blaudez, D. Ph.D. Thesis, Bordeaux I University, 1993.